Available online at www.sciencedirect.com
ScienceDirect
Trans. Nonferrous Met. Soc. China 35(2025) 921−931
Transactions of Nonferrous Metals Society of China
www.tnmsc.cn

Fabrication of Ti/SnO_x/MnO_2 anodes with enhanced catalytic performance for oxygen evolution reactions

Ya CHEN, Yuan-he JIANG, Peng-hui PING, Jiu-qing LIU, Xi-chang SHI

School of Metallurgy and Environment, Central South University, Changsha 410083, China

Received 11 July 2023; accepted 29 March 2024

Abstract: This work is devoted to the development of a low cost dimensionally stable anode with high oxygen evolution catalytic activity for practical applications. For this purpose, a Ti/SnO_x/MnO_2 anode was fabricated through an innovative strategy involving Sn electrodeposition, oxidation, and MnO_2-layer preparation. The structure of the anode was characterized, and the oxygen evolution performance was evaluated in a H_2SO_4 solution. The results show that compared with the Ti/SnO_2/MnO_2 anode prepared by the conventional brushing−annealing process, the Ti/SnO_x/MnO_2 anode fabricated through the innovative procedure exhibits a lower oxygen evolution potential and a nearly 40% longer accelerated lifespan. The superior oxygen evolution performance of the Ti/SnO_x/MnO_2 anode is attributed to the distinctive SnO_x intermediate layer fabricated through Sn electrodeposition followed by oxidation, which indicates the great potential of the anode as a dimensionally stable anode for metal electrowinning and hydrogen production by electrolysis, etc.

Key words: dimensionally stable anode; oxygen evolution catalytic performance; SnO_2 intermediate layer; MnO_2 catalyst

1 Introduction

In the past decades, dimensionally stable anodes (DSAs) with catalyst coatings have been applied in many industrial processes including metal electrowinning, sewage, and hydrogen production. Generally, the catalyst coating is fabricated on a titanium (Ti) substrate to catalyze the oxygen evolution reaction (OER) occurring at the anode−solution interface, and thus reduce the cell voltage and power consumption [1]. For this purpose, some noble metal oxides, especially IrO_2 and RuO_2, have been successfully used as the catalyst. Nevertheless, the high cost and limited-service life of the noble metal oxide coatings hinder their applications in some industrial areas [2,3]. Therefore, it is still a challenge to develop an OER catalyst coating with high catalytic activity and low cost to meet the requirement of these practical applications.

As a cheap transition metal oxide catalyst for DSAs, MnO_2 has attracted much attention in recent years due to its numerous advantages [4−7]. However, because of differences in lattice structures and thermal expansion coefficients between MnO_2 coatings and Ti substrates, significant cracks occur in the MnO_2 coating when a Ti/MnO_2 DSA is fabricated, which often result in the coating peeling and passivation of the Ti substrate in the following electrolysis test. To overcome this shortcoming, a basic approach is to introduce an intermediate oxide layer between the Ti substrate and the MnO_2 coating [8−10]. Tin dioxide (SnO_2) was frequently employed as the intermediate oxide due to its merits of strong binding and good conductivity [11−13]. In

Corresponding author: Ya CHEN, Tel: +86-18073101449, E-mail: chenya_mes@csu.edu.cn
DOI: https://doi.org/10.1016/S1003-6326(24)66723-3

most cases, the intermediate SnO_2 layer was created by applying a Sn-containing solution (or gel) onto the Ti substrate through brushing, followed by annealing at a high temperature [14]. Although the intermediate SnO_2 indeed can, to some extent, prolong the service time of the anode, it seems difficult for the Ti/SnO_2/MnO_2 DSA fabricated by the brushing−annealing process to satisfy the service-life requirement of industrial applications. Clearly, effective fabrication procedures are needed to further enhance the intimate contact of the MnO_2 coating/SnO_2 intermediate layer/Ti substrate, which is expected to improve the mechanical integrity and corrosion resistance of the DSA.

In this work, an innovative strategy to fabricate a Ti/SnO_x/MnO_2 anode was presented. The SnO_x intermediate layer of the anode was fabricated via Sn electrodeposition followed by oxidation, while the MnO_2 coating was prepared by a brushing−annealing method. After preliminary structural optimization, the obtained anode exhibited outstanding stability and excellent OER catalytic activity compared with the Ti/SnO_2/MnO_2 anode prepared by a conventional brushing−annealing process.

2 Experimental

2.1 Materials and reagents

Sulfuric acid (H_2SO_4, 98 wt.%) and oxalic acid ($H_2C_2O_4$) were obtained from Chengdu Chron Chemical Co., Ltd., China. Nickel chloride ($NiCl_2$), potassium permanganate ($KMnO_4$), boric acid (H_3BO_3), stannous sulfate ($SnSO_4$), sodium hydroxide (NaOH), and manganese nitrate ($Mn(NO_3)_2$) were purchased from Shanghai Wokai Biotechnology Co., Ltd., China and Sinopharm Chemical Reagent Co., Ltd., China. All chemical reagents were of analytical grade and were used without further purification. Titanium (Ti) plates were purchased from Xingwei Metal Technology Materials Co., Ltd., China.

2.2 Preparation of Ti/SnO_x/MnO_2 anodes

Ti plates were polished with 800-grit silicon carbide sand paper to remove the superficial dirt and oxide, and then cut into strips of 10 mm × 40 mm. After being degreased in a 2.5 mol/L NaOH solution at 90 °C for 1 h, the strips were further etched in a 0.5 mol/L $H_2C_2O_4$ solution at 90 °C for 1 h, and then rinsed with deionized water.

A Sn coating was electrodeposited on the Ti substrate. In order to improve the adhesion between the Sn coating and the Ti substrate, Ni was first electrodeposited on the Ti substrate from a mixed solution of 0.5 mol/L $NiCl_2$ and 0.5 mol/L H_3BO_3 before Sn deposition. After 900 s of Ni deposition, the Ti substrate with a thin Ni coating was subjected to Sn deposition and rinse. It was found that without the Ni intermediate deposition, the Sn coating fell off the Ti substrate during washing, and thus it was difficult to obtain a well-distributed and dense Sn coating on the Ti substrate. The current density for both Ni and Sn deposition was 5 mA/cm^2, but the electrolyte for Sn deposition was a mixed solution of 0.1 mol/L $SnSO_4$, 2 mol/L H_2SO_4, and 0.3 mol/L phenol. To optimize the structure of the Ti/SnO_x/MnO_2 anode, Sn coatings were prepared under different deposition durations, and then oxidized into SnO_x by soaking in $KMnO_4$ solutions with different pH for 20 h. The pH value of $KMnO_4$ solutions was adjusted using a H_2SO_4 solution and a NaOH solution, and was detected by a pH meter. The brown MnO_2 residue on the Ti/SnO_x surface resulted from the oxidation process was removed using a 0.1 mol/L $H_2C_2O_4$ solution. For fabricating a Ti/SnO_x/MnO_2 anode, the Sn oxide coating on the Ti substrate was finally brushed with an aqueous manganese nitrate solution with a concentration of 50 wt.%, and annealed at 300 °C for 30 min. This brushing−annealing process was repeated ten times.

2.3 Physical characterization

The crystallographic structure of the coating was tested through X-ray diffraction (XRD, Rint−2000, Rigaku Corporation, using Cu K_α radiation). The morphology was characterized through field emission scanning electron microscopy (FESEM, Nova NanoSEM230). The elemental valence state was studied by X-ray photoelectron spectrophotometry (XPS, Thermo Scientific, ESCALAB 250 Xi) with Al K_α radiation.

2.4 Electrochemical measurements

All electrochemical measurements were carried out at room temperature using a three-electrode system in conjunction with a CHI660E electrochemical workstation. The fabricated Ti/SnO_x/MnO_2 electrode, titanium mesh, and a saturated

mercury−mercurous sulfate electrode (MSE) were applied as the working, auxiliary, and reference electrodes in the system, respectively. The working electrode and auxiliary electrode were positioned 3 cm apart, and the electrolyte was a mixed solution with 1 mol/L Na_2SO_4 and 0.25 mol/L H_2SO_4. Na_2SO_4 was used as the supporting electrolyte in order to increase the overall concentration of the electrolyte and eliminate the diffuse-layer effect. The oxygen evolution potential (OEP) and Tafel slope were measured by linear sweep voltammetry (LSV) tests, which were conducted between 0.6 and 1.4 V at a scanning rate of 2 mV/s. To determine the electrochemical active surface area (ECSA) of the DSA, cyclic voltammetry (CV) curves were recorded from 0.55 to 0.65 V at the scanning rates from 2 to 10 mV/s. The EIS test was carried out in the frequency range from 100 kHz to 10 mHz with an initial potential of 1 V and an amplitude of 5 mV.

2.5 Accelerated lifespan tests

A two-electrode setup coupled to an electrochemical workstation CHI660E was applied to conducting the accelerated lifespan test at room temperature. The Ti/SnO_x/MnO_2 electrode to be measured was used as the working electrode, and titanium mesh was used as the auxiliary electrode. The spacing between them was fixed to be 3 cm. The current density was set to be 250 mA/cm^2, and the electrolyte was 0.5 mol/L H_2SO_4. The electrode was deemed to be invalid when the cell voltage surpassed 10 V.

3 Results and discussion

3.1 Microstructural features of fabricated Ti/SnO_x/MnO_2 anode

The surface morphologies of the substrate and coatings were characterized by SEM. As presented in Figs. 1(a) and (b), the smooth surface of the Ti substrate can be converted into porous one by pretreatment in a $H_2C_2O_4$ solution, which is beneficial to the cohesion of the substrate and coatings. Figures 1(c) and (d) show the SEM images of the Ni and Sn coatings created by electrodeposition, respectively. The smooth and compact morphologies suggest that the pores of the Ti substrate are filled with Ni and Sn.

The compact feature of the coating can be further confirmed by the SEM image and EDS mapping of the cross-section presented in Figs. 2(a) and (b). The dense coating is expected to block oxygen penetration, thus preventing the formation of high-resistance TiO_2 on the Ti substrate during the OER. After oxidation in a $KMnO_4$ solution (0.05 mol/L $KMnO_4$ and 0.05 mol/L H_2SO_4), the

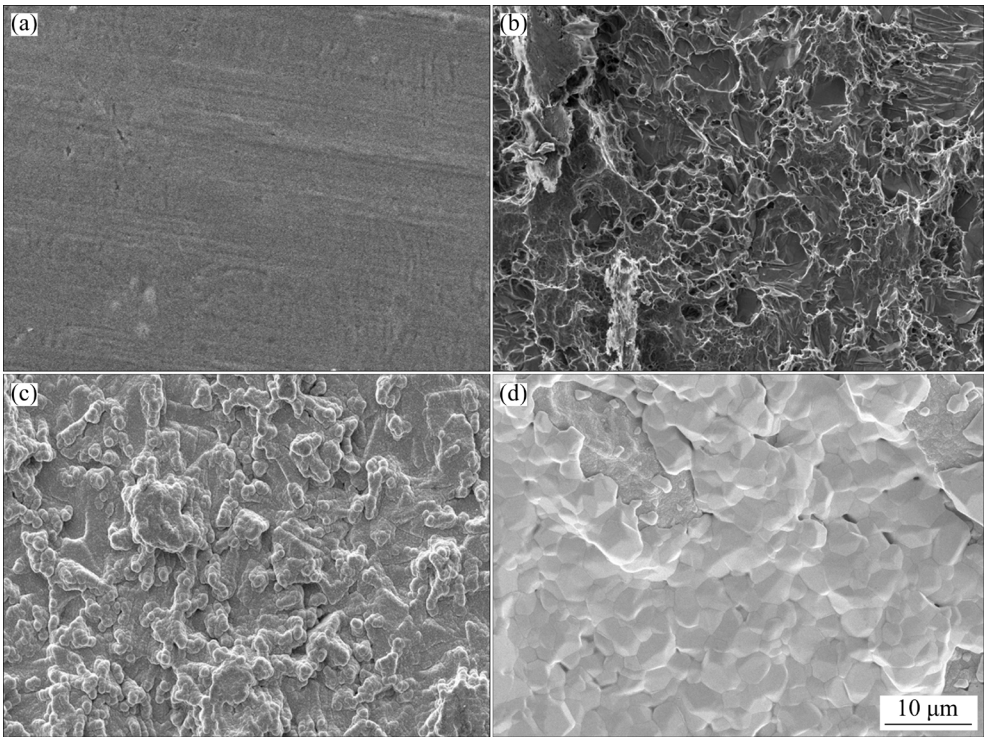

Fig. 1 SEM images of Ti substrate before (a) and after (b) pretreatment, Ni coating (c), and Sn coating (d)

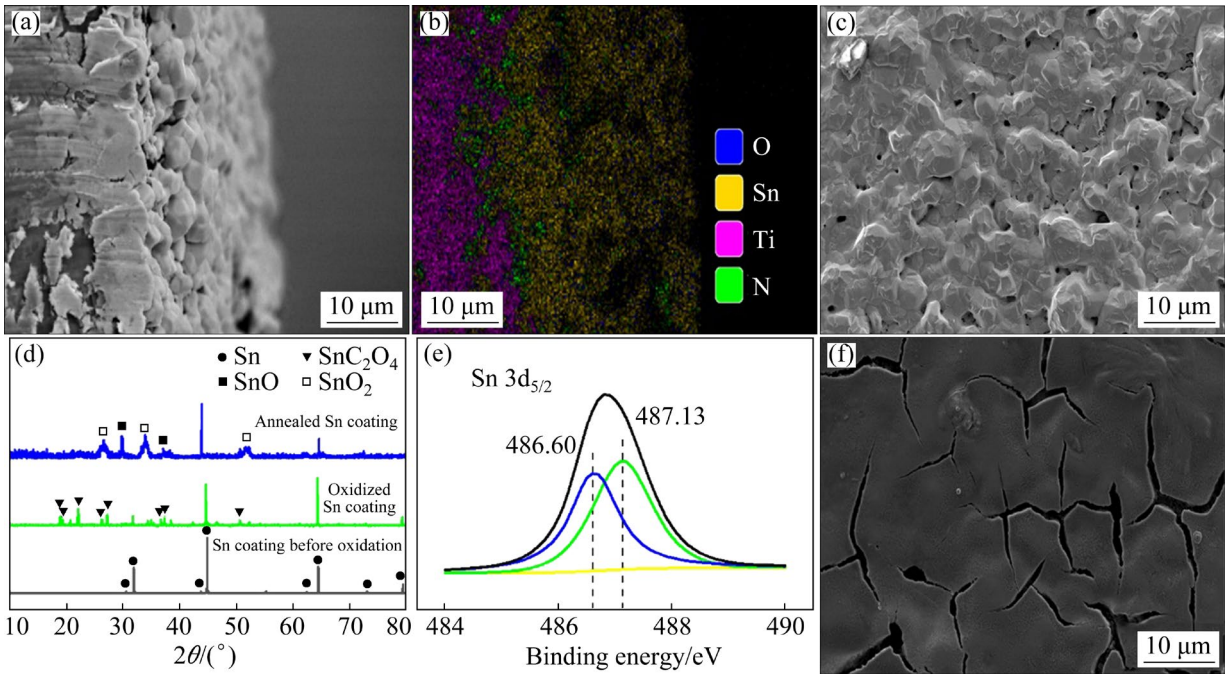

Fig. 2 SEM image (a) and EDS mapping (b) of cross-section of Ti substrate with Ni and Sn coatings, SEM image of oxidized Sn coating (c), XRD patterns of Sn coating, SnO_x after oxidization in $KMnO_4$ solution and annealing in air (d), XPS spectra of oxidized Sn coating (e), and SEM image of MnO_2 layer on oxidized Sn coating (f)

oxidized Sn coating exhibits a somewhat rough surface (Fig. 2(c)). The rough oxide surface should facilitate the cohesion of the intermediate layer and MnO_2 layer, thus enhancing the service life of the electrode.

To ascertain the phase composition, the crystal structure information of the Sn coating before and after oxidation was collected by XRD (Fig. 2(d)). The XRD pattern of the coating before oxidation presents peaks at 2θ values of 30.6°, 32.0°, 44.9°, 62.5°, 64.6°, 73.2°, and 79.5°, which are all indexed to Sn (JCPDS No.86-2264) (the bottom pattern in Fig. 2(d)). After being oxidized in the $KMnO_4$ solution and treated with oxalic acid, the coating reveals characteristic diffraction peaks of SnC_2O_4 (JCPDS No.50-1429) and SnO_2 (JCPDS No.41-1445) (the middle pattern in Fig. 2(d)), suggesting that the $KMnO_4$ solution can at least partially oxidize the Sn coating into oxides. To investigate the effect of the follow-up annealing on the composition of the oxidized Sn coating, the coating was annealed in air at 300 °C for 5 h, and then characterized by XRD (the top pattern in Fig. 2(d)). The peaks at 2θ values of 26.6°, 33.9°, 51.8° and 29.9°, 33.3° are indexed to SnO_2 (JCPDS No.41-1445) and SnO (JCPDS No.85-0423), respectively. In addition, peaks related to Sn can also be detected after annealing, suggesting that the Sn coating cannot fully convert into SnO_x even after the annealing process. However, given that the Sn and SnO can both combine with oxygen penetrating from the outer MnO_2 layer, the incompletely oxidized Sn intermediate layer is at least able to block the oxygen penetration, thus alleviating the corrosion of the Ti substrate at the early stage of OER. The diffraction peaks of titanium and nickel on the substrate are undetectable, indicating a thick and compact Sn coating.

The elemental valence state of the oxidized Sn coating was determined by XPS, and Fig. 2(e) presents the spectrum of Sn $3d_{5/2}$. The two peaks at 486.60 and 487.13 eV correspond to the binding energy of SnO and SnO_2, respectively [15,16], in agreement with the XRD result. Peaks related to Sn metal are absent in the spectrum, implying the occurrence of Sn oxidation on the surface and in the subsurface layer of the Sn coating. Figure 2(f) shows the typical surface morphology of the catalytic MnO_2 coating prepared by the brushing−annealing process. Although the MnO_2 coating was fabricated upon the oxidized Sn intermediate layer, a few cracks inevitably developed in the coating

during the annealing process. An effective procedure is still needed for fabricating a crack-free MnO_2 layer with high OER performance.

3.2 Electrochemical performance of fabricated Ti/SnO_x/MnO_2 anode

The oxygen evolution electrocatalytic performance of the Ti/SnO_x/MnO_2 anode was evaluated by LSV and EIS tests in a mixed solution of 1 mol/L Na_2SO_4 and 0.25 mol/L H_2SO_4. To optimize the OER performance of the electrodes, Ti/SnO_x/MnO_2 anodes fabricated with different Sn electrodeposition durations were subjected to LSV tests, and the obtained curves are displayed in Fig. 3(a). Each LSV curve presents a small response current in the low potential range, and a rapid current increase in the high potential range due to the occurrence of the OER. For comparing the OER activity of the anodes with different Sn electrodeposition durations, the oxygen evolution potential (OEP) at a polarization current density of 10 mA/cm^2 and the corresponding over-potential (η) were calculated based on the LSV curves. The results in Table 1 show that the anode fabricated with 500 s of Sn electrodeposition has the lowest OEP (1.025 V), suggesting that too thick or thin Sn coatings may lead to a high OEP.

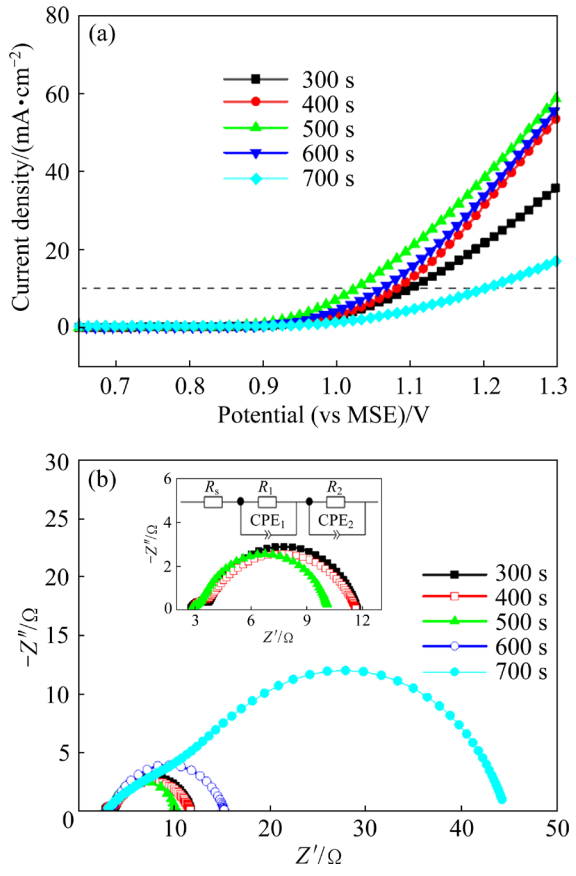

Fig. 3 LSV curves (a) and EIS data (b) of Ti/SnO_x/MnO_2 anodes fabricated with different Sn electrodeposition durations

Table 1 OEP and η of Ti/SnO_x/MnO_2 anodes fabricated with different Sn electrodeposition durations

Deposition time/s	OEP (vs MSE)/V	η (vs MSE)/V
300	1.100	0.558
400	1.082	0.540
500	1.025	0.483
600	1.061	0.519
700	1.202	0.660

Generally speaking, an electrochemical reaction preferentially occurs on the active sites of the electrode−electrolyte interface, to (or from) which electronics and electrochemical active species can be facilely transported from (or to) the outer circuit and electrolyte, respectively. In the case of short Sn electrodeposition durations, it is postulated that the thin Sn coating is not fully able to protect the Ti substrate oxidation during $KMnO_4$ oxidation and annealing processes. The partially oxidized Ti substrate should influence electronic transportation between the electrode−electrolyte interface and external circuitry, thus reducing the active site or active area of the electrode catalyst layer. Since the electrodes were fabricated with long Sn electrodeposition durations, the high OEP may result from their too thick Sn oxide coatings, which contain a certain amount of low conductive Sn oxide (SnO).

Figure 3(b) shows the Nyquist plots of the anodes fabricated with various Sn electrodeposition durations. Unlike those collected on precious metal oxide catalysts, each of the plots demonstrates two semicircles (arcs), of which the small semicircle (arc) in the higher frequency range is believed to derive from the electrode process (corrosion of the substrate) occurring in the micro-pores of the catalyst layer, while the large one in the lower frequency range is ascribed to the OER process occurring at the electrode−electrolyte interface [17,18]. For the Ti/SnO_x/MnO_2 anode, since the Ti substrate is covered by a partially-oxidized Sn coating, the small arc should be related to the corrosion of Sn or Ti substrate. The diameter of the semicircle (arc) denotes the charge transfer resistance of the corresponding electrode process,

and the intersection of the Z' axis and the curve at the high frequency end represents the ohmic resistance of the entire electrode system (including the electrolyte, electrode material, and external circuitry) [19−22].

The EIS data were fitted by using the equivalent circuit in the inset of Fig. 3(b), and the obtained corrosion-related resistance (R_1) and OER charge transfer resistance (R_2) of the anodes are displayed in Table 2. The anode fabricated with 500 s of Sn electrodeposition exhibits the lowest OER resistance (R_2=6.826 Ω), which is in good agreement with the LSV measurements, and further demonstrates that the anode fabricated with 500 s of Sn electrodeposition has the best electrochemical performance. The anode with 700 s of Sn electrodeposition shows a much higher R_1 value compared with the other ones, suggesting this thick tin oxide coatings can prevent the inner Sn or Ti from corrosion. The relatively high R_1 of anodes with short Sn electrodeposition durations should be attributed to the partially-oxidized Ti substrate as mentioned above.

Table 2 Equivalent circuit parameters of anodes fabricated with different Sn electrodeposition durations

Deposition time/s	R_1/Ω	R_2/Ω
300	0.944	8.029
400	0.699	8.060
500	0.587	6.826
600	0.498	11.78
700	12.69	29.25

Given that the oxidation activity of $KMnO_4$ solutions used for oxidizing Sn intermediate layers depends on the acidity, the effect of the initial pH of $KMnO_4$ solutions on the OER performance of the fabricated Ti/SnO_x/MnO_2 anodes was also investigated. For convenience, the initial pH values, −0.004, 0.509, 0.965, and 1.241 are denoted as pH1, pH2, pH3, and pH4, respectively. Figure 4 shows the LSV and accelerated lifespan curves of the anodes fabricated after oxidation in $KMnO_4$ solutions with different initial pH values. As can be observed, all anodes have relatively low OEPs, with the exception of the one oxidized under pH1, which has a noticeably larger OEP. The accelerated lifespan test result shows a significant decrease in electrode service life with increasing oxidant acidity.

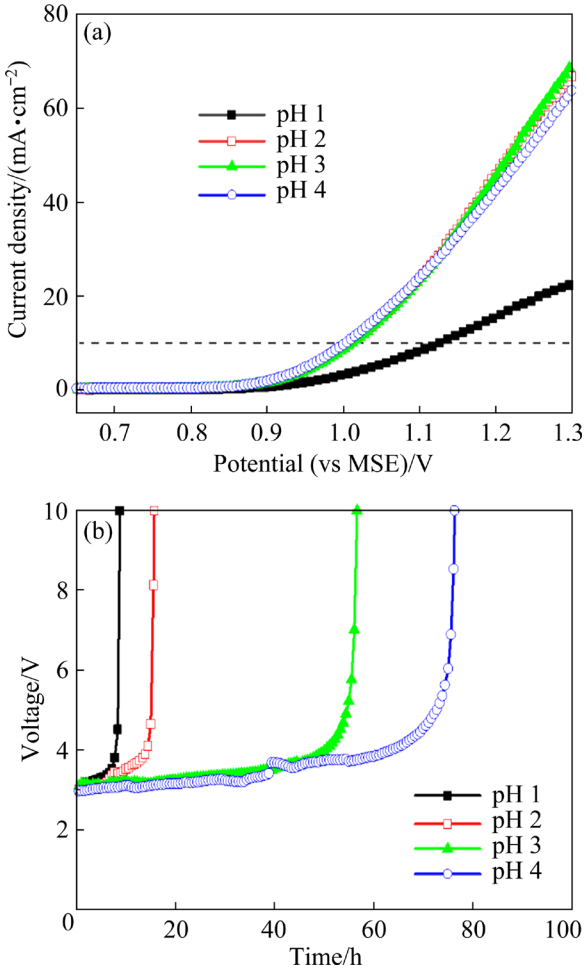

Fig. 4 LSV (a) and accelerated lifespan (b) curves of Ti/SnO_x/MnO_2 anodes fabricated after oxidation in $KMnO_4$ solutions with different initial pH values

It is postulated that the high acidity of $KMnO_4$ solutions leads to the serious dissolution of the Sn intermediate, which affects the protective effect of the produced tin oxide intermediate layer. As a result, the Ti substrate is exposed to the strong oxidizing $KMnO_4$ solution, and the passivation of the substrate results in the high OEP and short service life of the fabricated Ti/SnO_x/MnO_2 electrode. These results suggest that controlling the $KMnO_4$ solution to a weak acidity range can effectively enhance the service life of the Ti/SnO_x/MnO_2 anode. However, further investigation demonstrates that increasing the pH of $KMnO_4$ solutions from 1.241 to about 5 has little effect on the OEP and service life of the anode (the data are not presented here).

To verify the superiority of the proposed Ti/SnO_x/MnO_2 anode, a Ti/MnO_2 anode without intermediate layers and a Ti/SnO_2/MnO_2 anode with

SnO_2 intermediate layer prepared by the conventional brushing−annealing process were fabricated. The pretreatment of Ti substrates and the preparation of MnO_2 layers were carried out with reference to the procedures described in the experimental section. A Sn-containing solution with 10 g $SnCl_2·2H_2O$ in 50 mL ethanol was uniformly brushed on the Ti substrate and then annealed at 500 °C for 1 h. The brushing−annealing process was repeated four times to ensure the same intermediate layer thickness of the Ti/SnO_2/MnO_2 and Ti/SnO_x/MnO_2 electrodes. For comparison, the Ti/MnO_2, Ti/SnO_2/MnO_2, and Ti/SnO_x/MnO_2 electrodes were denoted as E1, E2, and E3, respectively, and all were subjected to electrochemical tests under the same conditions.

Figure 5(a) presents the LSV curves of the electrodes with and without SnO_2 intermediate layers. At a current density of 10 mA/cm^2, the E3 electrode demonstrates a much lower OEP compared to the E1 and E2 electrodes, while the E2 electrode exhibits just a little improvement in OEP relative to the E1. The kinetics of the OER can be analyzed based on the Tafel formula:

$$\eta = -\frac{2.3RT}{\alpha F}\lg J_0 + \frac{2.3RT}{\alpha F}\lg J \quad (1)$$

where R is the molar gas constant, T is the thermodynamic temperature, α is the transfer coefficient, F is the Faraday constant, J_0 and J are the exchange current density and current density of the electrode, respectively. As shown in Fig. 5(b), the E3 electrode exhibits a much lower Tafel slope (b=2.3RT/(αF)) than the other two electrodes.

It is well recognized that the OER is a four-step reaction with a single electron transfer occurring at each step, and M—OH, M—O, and M—OOH are formed before oxygen evolution [23−26]. The slowest step in the OER process is the rate-determining step (RDS), which determines the rate of the whole reaction [27,28]. Since the repetition of RDS is 1 in the whole OER process, the value of the transfer coefficient (α) should equal the sum of the symmetry coefficient of RDS and the number of electrons transmitted prior to the RDS [29]. According to the calculations in Fig. 5(b), the nominal α values of E1, E2, and E3 electrodes are 0.194, 0.213, and 0.417, respectively, which indicates that the M—O generation reaction is the RDS in the three electrodes.

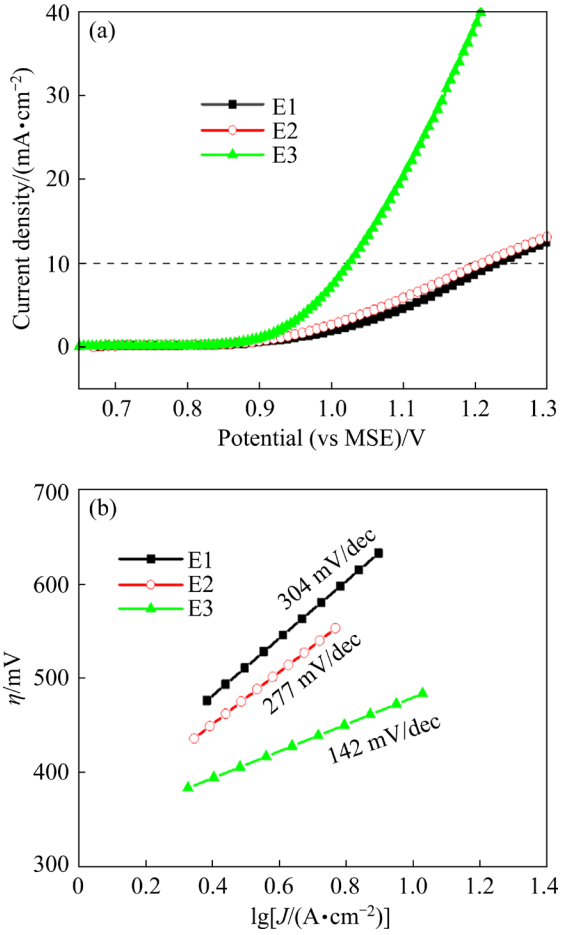

Fig. 5 LSV curves (a) and Tafel slopes (b) of DSAs with and without SnO_2 interlayers

Considering that the electrochemically active surface area is positively correlated with the double layer capacitance (C_{dl}) of electrodes [30,31], CV curves were tested and the C_{dl} values of the electrodes were calculated according to the procedure reported in Refs. [32,33]. Figures 6(a−c) present the CV curves, and Fig. 6(d) shows the current density difference vs scan rate based on the CV curves, and the calculated C_{dl} of the E1, E2, and E3 electrodes. The C_{dl} of the E3 electrode is 19.27 mF/cm^2, which is about three times that of the E1 electrode and twice that of the E2 electrode, suggesting a much higher electrochemical active surface area.

The difference in electrochemical active sites can be further confirmed by the EIS data of the electrodes (Fig. 7). The EIS data were fitted by using the equivalent circuit in Fig. 3(b), and the results are listed in Table 3. The relatively high R_1 of the E1 electrode can be attributed to the absence of intermediate layers on the Ti substrate, which led

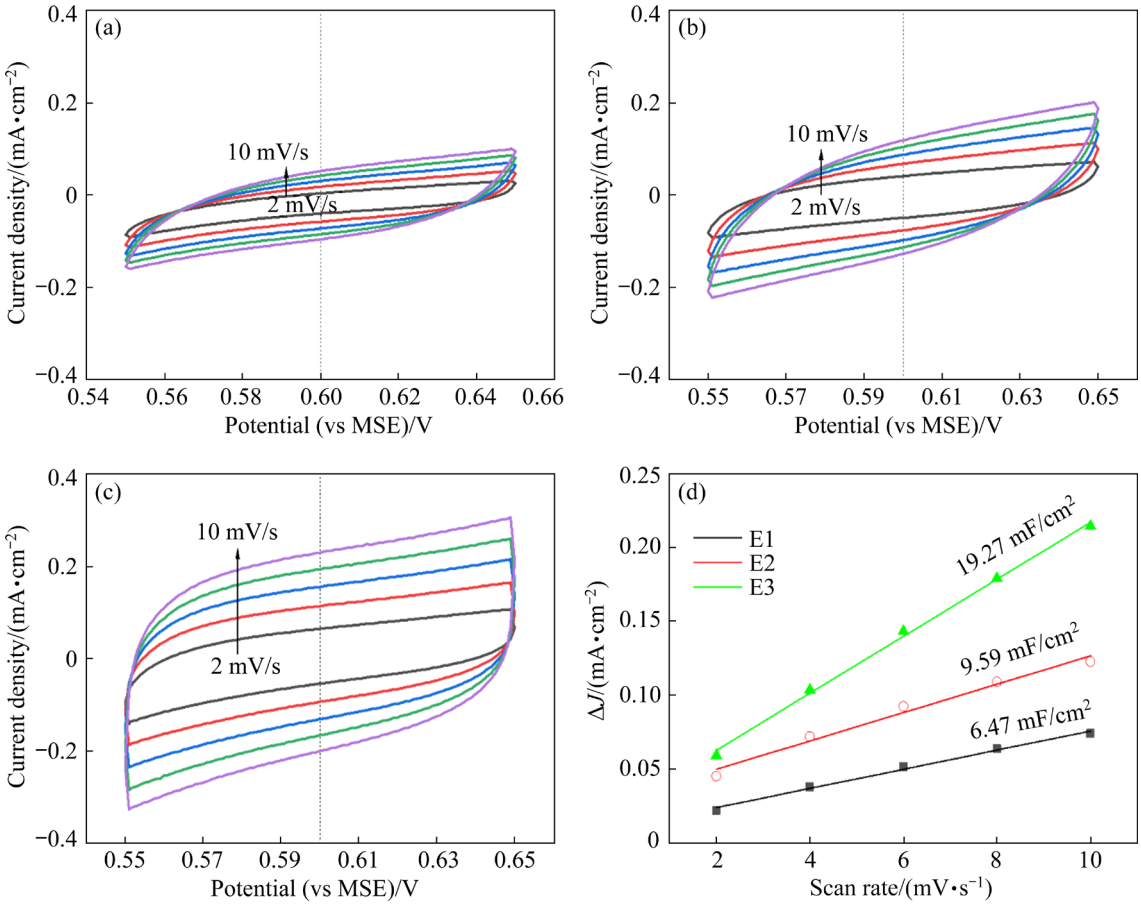

Fig. 6 CV curves of E1 (a), E2 (b), and E3 (c) electrodes, and current density difference vs scan rate based on CV curves (d)

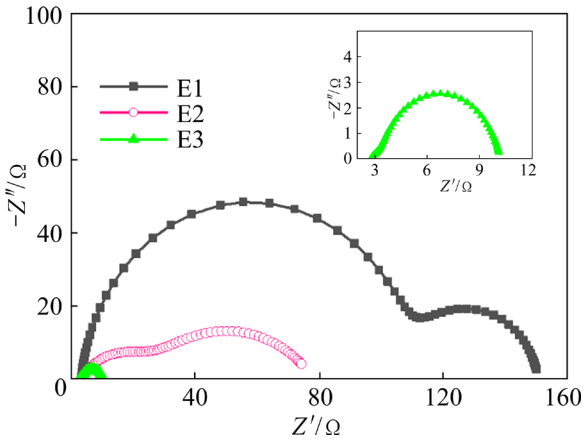

Fig. 7 EIS data of E1, E2 and E3 electrodes

Table 3 Equivalent circuit parameters of E1, E2 and E3 electrodes

Electrode	R_1/Ω	R_2/Ω
E1	106.7	40.78
E2	21.87	52.85
E3	0.587	6.826

to a TiO_2 passivation layer on the substrate during the annealing process [21]. For the E2 and E3 electrodes, the intermediate layers to different extents protect the Ti substrate from oxidation, and result in a prominent reduction of R_1. Compared with E1 and E2 electrodes, the E3 electrode exhibits the lowest charge transfer resistance (R_2), which illustrates its rich electrochemical active sites and excellent OER performance. As mentioned above, the SnO_x intermediate layer fabricated by electro-deposition followed by oxidation can act as effective protection for the Ti substrate, which facilitates the electronic transportation between the electrode−electrolyte interface and external circuitry, thus increasing the electrochemical active site of the MnO_2 layer. Conversely, the oxidation of the substrate should affect the electron transport, and increase the dead mass of MnO_2.

Additionally, the above results are also reflected in the accelerated lifespan test (Fig. 8). The E1 electrode without intermediate layers is rapidly deactivated by passivation under high

current densities. The accelerated lifespan of the E2 and E3 electrodes can reach 55 and 76 h, respectively. A nearly 40% longer accelerated lifespan further demonstrates that the SnO_x intermediate layer prepared by the novel method has superior resistance to passivation.

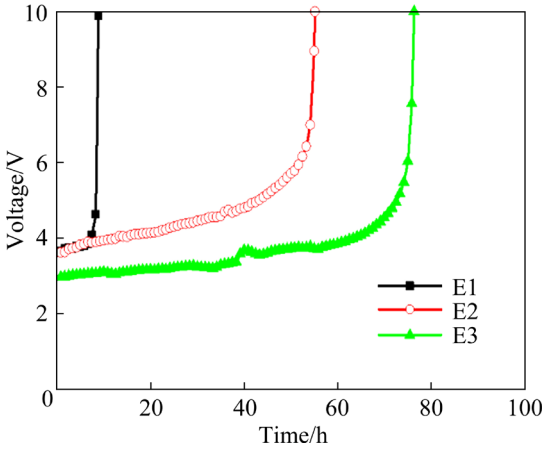

Fig. 8 Accelerated lifespan curves of E1, E2 and E3 electrodes

4 Conclusions

(1) An innovative strategy, which involves Sn electrodeposition, oxidation, and MnO_2 layer preparation, was proposed to fabricate a Ti/SnO_x/MnO_2 anode with the enhanced catalytic performance.

(2) The structure of the Ti/SnO_x/MnO_2 anode was optimized, and the anode fabricated with 500 s of Sn electrodeposition shows superior OER performance.

(3) Compared with the Ti/SnO_2/MnO_2 anode prepared by a conventional brushing−annealing process, the fabricated Ti/SnO_x/MnO_2 anode exhibits a lower OER potential, nearly 40% longer accelerated lifespan, and great application potential in metal electrowinning, hydrogen production, etc.

CRediT authorship contribution statement

Ya CHEN: Conceptualization, Methodology, Funding acquisition, Writing – Original draft; **Yuan-he JIANG:** Investigation, Data curation; **Jiu-qing LIU:** Formal analysis; **Peng-hui PING** and **Xi-chang SHI:** Methodology.

Declaration of competing interest

The authors declare that they have no known competing financial interests or personal relationships that could have appeared to influence the work reported in this paper.

References

[1] VAZHAYIL A, VAZHAYAL L, THOMAS J, ASHOK C S, THOMAS N. A comprehensive review on the recent developments in transition metal-based electrocatalysts for oxygen evolution reaction [J]. Applied Surface Science Advances, 2021, 6: 100184.

[2] DUAN Ran, LI Ye-jun, WANG Shu, TONG Yong-gang, RUBAHN H G, ZHANG Gu-fei, QI Wei-hong. Effects of phosphate precursors on morphology and oxygen evolution reaction activity of NiFe (oxy)hydroxide on nickel foams [J]. Transactions of Nonferrous Metals Society of China, 2022, 32(12): 4050−4061.

[3] YU Le, YANG Jing-fan, GUAN Bu-yuan, LU Yan, LOU Xiong-wen. Hierarchical hollow nanoprisms based on ultrathin Ni−Fe layered double hydroxide nanosheets with enhanced electrocatalytic activity towards oxygen evolution [J]. Angewandte Chemie: International Edition, 2018, 57(1): 172−176.

[4] AL-OWEINI R, SARTOREL A, BASSIL B S, NATALI M, BERARDI S, SCANDOLA F, KORTZ U, BONCHIO M. Photocatalytic water oxidation by a mixed-valent $Mn^{III}_3Mn^{IV}O_3$ manganese oxo core that mimics the natural oxygen-evolving center [J]. Angewandte Chemie−International Edition, 2014, 53(42): 11182−11185.

[5] FRYDENDAL R, PAOLI E A, CHORKENDORFF I, ROSSMEISL J, STEPHENS I E L. Toward an active and stable catalyst for oxygen evolution in acidic media: Ti-stabilized MnO_2 [J]. Advanced Energy Materials, 2015, 5(22): 1500991.

[6] HE Jun-kai, WANG Ming-chao, WANG Wen-bo, MIAO Ran, ZHONG Wei, CHEN Sheng-yu, POGES S, JAFARI T, SONG Wen-qiao, LIU Jia-chen, SUIB S L. Hierarchical mesoporous NiO/MnO_2@PANI core–shell microspheres, highly efficient and stable bifunctional electrocatalysts for oxygen evolution and reduction reactions [J]. ACS Applied Materials & Interfaces, 2017, 9(49): 42676−42687.

[7] HUYNH M, BEDIAKO D K, NOCERA D G. A functionally stable manganese oxide oxygen evolution catalyst in acid [J]. Journal of the American Chemical Society, 2014, 136(16): 6002−6010.

[8] PIERCY B, ALLEN C, GULLÁ A F. Ta and Ti anti-passivation interlayers for oxygen-evolving anodes produced by cold gas spray [J]. Journal of Thermal Spray Technology, 2015, 24(4): 702−710.

[9] SHAO Dan, YAN Wei, CAO Lu, LI Xiao-liang, XU Hao. High-performance Ti/Sb−SnO_2/Pb_3O_4 electrodes for chlorine evolution: Preparation and characteristics [J]. Journal of Hazardous Materials, 2014, 267: 238−244.

[10] XU Hai-bo, LU Yong-hong, LI Chun-hui, HU Jie-zhen. A novel IrO_2 electrode with iridium–titanium oxide interlayers from a mixture of TiN nanoparticle and H_2IrCl_6 solution [J]. Journal of Applied Electrochemistry, 2010, 40(4): 719−727.

[11] MARTÍNEZ-HUITLE C A, BRILLAS E. Decontamination of wastewaters containing synthetic organic dyes by electrochemical methods: A general review [J]. Applied Catalysis B: Environmental, 2009, 87(3/4): 105−145.

[12] PANIZZA M, CERISOLA G. Direct and mediated anodic oxidation of organic pollutants [J]. Chemical Reviews, 2009, 109(12): 6541−6569.

[13] ZHAO Guo-hua, CUI Xiao, LIU Mei-chuan, LI Pei-qiang, ZHANG Yong-gang, CAO Tong-cheng, LI Hong-xu, LEI Yan-zhu, LIU Lei, LI Dong-ming. Electrochemical degradation of refractory pollutant using a novel micro-structured TiO_2 nanotubes/Sb-doped SnO_2 electrode [J]. Environmental Science & Technology, 2009, 43(5): 1480−1486.

[14] CHEN Xin, GUO Hua-jun, LUO Shu-liang, WANG Zhi-xing, LI Xin-hai. Effect of SnO_2 intermediate layer on performance of Ti/SnO_2/MnO_2 electrode during electrolytic-manganese process [J]. Transactions of Nonferrous Metals Society of China, 2017, 27(6): 1417−1422.

[15] DI GIULIO M, SERRA A, TEPORE A, RELLA R, SICILIANO P, MIRENGHI L. Influence of the deposition parameters on the physical properties of tin oxide thin films [J]. Materials Science Forum, 1996, 203: 143−148.

[16] GRUTSCH P A, ZELLER M V, FEHLNER T P. Photoelectron spectroscopy of tin compounds [J]. Inorganic Chemistry, 1973, 12(6): 1431−1433.

[17] HU J M, MENG H M, ZHANG J Q, CAO C N. Degradation mechanism of long service life Ti/IrO_2−Ta_2O_5 oxide anodes in sulphuric acid [J]. Corrosion Science, 2002, 44(8): 1655−1668.

[18] DA SILVA L M, DE FARIA L A, BOODTS J F C. Electrochemical impedance spectroscopic (EIS) investigation of the deactivation mechanism, surface and electrocatalytic properties of Ti/RuO_2(x)+Co_3O_4(1−x) electrodes [J]. Journal of Electroanalytical Chemistry, 2002, 532(1/2): 141−150.

[19] CHAKTHRANONT P, KIBSGAARD J, GALLO A, PARK J, MITANI M, SOKARAS D, KROLL T, SINCLAIR R, MOGENSEN M B, JARAMILLO T F. Effects of gold substrates on the intrinsic and extrinsic activity of high-loading nickel-based oxyhydroxide oxygen evolution catalysts [J]. ACS Catalysis, 2017, 7(8): 5399−5409.

[20] LYONS M E G, BRANDON M P. The significance of electrochemical impedance spectra recorded during active oxygen evolution for oxide covered Ni, Co and Fe electrodes in alkaline solution [J]. Journal of Electroanalytical Chemistry, 2009, 631(1/2): 62−70.

[21] ZHANG C J, BERLINGUETTE C P, TRUDEL S. Water oxidation catalysis: An amorphous quaternary Ba−Sr−Co−Fe oxide as a promising electrocatalyst for the oxygen-evolution reaction [J]. Chemical Communications, 2016, 52(7): 1513−1516.

[22] LUKIĆ Z, HEITMANN K, HABIB S, BASHINSKY S, RICKER P M. The halo mass function: High-redshift evolution and universality [J]. The Astrophysical Journal, 2007, 671(2): 1160−1181.

[23] KIM J S, KIM B, KIM H, KANG K. Recent progress on multimetal oxide catalysts for the oxygen evolution reaction [J]. Advanced Energy Materials, 2018, 8(11): 1702774.

[24] LI Lei-gang, WANG Peng-tang, SHAO Qi, HUANG Xiao-qing. Recent progress in advanced electrocatalyst design for acidic oxygen evolution reaction [J]. Advanced Materials, 2021, 33(50): e2004243.

[25] REIER T, NONG H N, TESCHNER D, SCHLÖGL R, STRASSER P. Electrocatalytic oxygen evolution reaction in acidic environments – Reaction mechanisms and catalysts [J]. Advanced Energy Materials, 2017, 7(1): 1601275.

[26] ROSSMEISL J, QU Z W, ZHU H, KROES G J, NØRSKOV J K. Electrolysis of water on oxide surfaces [J]. Journal of Electroanalytical Chemistry, 2007, 607(1/2): 83−89.

[27] ANANTHARAJ S, EDE S R, KARTHICK K, SAM SANKAR S, SANGEETHA K, KARTHIK P E, KUNDU S. Precision and correctness in the evaluation of electrocatalytic water splitting: Revisiting activity parameters with a critical assessment [J]. Energy & Environmental Science, 2018, 11(4): 744−771.

[28] IQBAL B, SALEEM M, ARSHAD S N, RASHID J, HUSSAIN N, ZAHEER M. One-pot synthesis of heterobimetallic metal–organic frameworks (MOFs) for multifunctional catalysis [J]. Chemistry, 2019, 25(44): 10490−10498.

[29] WU Zhi-peng, LU Xue-feng, ZANG Shuang-quan, LOU Xiong-wen. Non-noble-metal-based electrocatalysts toward the oxygen evolution reaction [J]. Advanced Functional Materials, 2020, 30(15): 1910274.

[30] ANANTHARAJ S, EDE S R, SAKTHIKUMAR K, KARTHICK K, MISHRA S, KUNDU S. Recent trends and perspectives in electrochemical water splitting with an emphasis on sulfide, selenide, and phosphide catalysts of Fe, Co, and Ni: A review [J]. ACS Catalysis, 2016, 6(12): 8069−8097.

[31] ANANTHARAJ S, KARTHICK K, KUNDU S. Evolution of layered double hydroxides (LDH) as high performance water oxidation electrocatalysts: A review with insights on structure, activity and mechanism [J]. Materials Today Energy, 2017, 6: 1−26.

[32] FUJIMOTO K, UEDA Y, INOHARA D, FUJII Y, NAKAYAMA M. Cobalt-doped electrolytic manganese dioxide as an efficient bifunctional catalyst for oxygen evolution/reduction reactions [J]. Electrochimica Acta, 2020, 354: 136592.

[33] HAN Guan-qun, LIU Yan-ru, HU Wen-hui, DONG Bin, LI Xiao, SHANG Xiao, CHAI Yong-ming, LIU Yun-qi, LIU Chen-guang. Crystallographic structure and morphology transformation of MnO_2 nanorods as efficient electro-catalysts for oxygen evolution reaction [J]. Journal of the Electrochemical Society, 2016, 163(2): H67−H73.

具有增强析氧催化性能 $Ti/SnO_x/MnO_2$ 阳极的制备

陈 亚，姜源鹤，平鹏辉，刘久清，石西昌

中南大学 冶金与环境学院，长沙 410083

摘 要：为了开发具有高析氧催化活性的低成本形稳阳极，提出一种包括 Sn 电沉积、沉积层氧化及 MnO_2 层制备等工艺过程的形稳阳极制备新方法，并将其用于制备 $Ti/SnO_x/MnO_2$ 阳极以进行材料结构表征以及在 H_2SO_4 溶液中进行析氧催化性能测试。结果表明，与采用传统刷涂−退火工艺制备的 $Ti/SnO_2/MnO_2$ 阳极相比，采用该新工艺制备的阳极具有更低的析氧电势，且加速测试寿命提高了近 40%。该阳极的优异性能得益于由 Sn 沉积层氧化转化而成的 SnO_x 中间层。该形稳阳极在金属电积及电解制氢等领域具有较大的应用潜力。

关键词：形稳阳极；析氧催化性能；氧化锡中间层；二氧化锰催化剂

(Edited by Wei-ping CHEN)